JOURNAL OF MATERIALS SCIENCE **35** (2000) 2499–2505

The interfacial reaction and microstructure in a ZK60-based hybrid composite

MINGYUAN GU*, ZHENGAN WU, YANPING JIN
State Key Laboratory of MMCs, Shanghai Jiao Tong University, Shanghai 200030, People's Republic of China
E-mail: mygu@fudan.ac.cn

MUSTAFA KOÇAK
GKSS Research Center, Institute of Materials Research, D-21502, Geesthacht, Germany

The oxidation behavior of B_4C particles was investigated by measuring the weight changes during isothermal heating at 650 to 800 °C. The interfacial microstructure and fractography of the B_4Cp and SiCw reinforced ZK60 magnesium hybrid composite was studied using a scanning electron microscope (SEM), a transmission electron microscope (TEM) and an electron energy loss spectrometer (EELS). It was found that the oxidation of B_4C particles in air at the temperatures investigated produced an amorphous B_2O_3 surface layer. The oxidation kinetics was limited by the diffusion rate of oxygen through the liquid B_2O_3 layer. The oxidation layer was found to dominate the interfacial reaction, the microstructure and the mechanical properties of the hybrid composite. The rod-like MgB_2 and the granular MgO were produced due to the reaction between the B_2O_3 and the magnesium matrix. The intimate bonding between the MgB_2 and both the reinforcements and the matrix is believed to be the main reason for the improvement of the mechanical properties of the composite.

1. Introduction

SiC whisker reinforced magnesium alloy composites are excellent constructional materials owing to their low density, high stiffness and strength to weight ratios, high thermal conductivity and high chemical compatibility between their reinforcements and matrix alloys [1, 2]. High costs of whiskers and health risks involved in the fabrication process, however, limit their applications. Alternatively, magnesium-based hybrid composites reinforced with a combination of short ceramic fibers and particles are developed in recent years [3, 4]. The addition of the particles into the short fiber preform was found not only to lower the costs but also to increase the isotropic properties of the composite [3]. B_4C is one of the particles often used as reinforcements in magnesium-based composites due to its lowest density and third highest hardness in ceramic materials and relatively low cost. In addition, it is stable enough in the matrix of magnesium [5]. However, B_4C is very prone to oxidation. Equation 1 is the most probable reaction course because the free energy of formation of B_2O_3 is the most negative relative to that of all other boron oxides [6, 7]. Therefore, in normal conditions, there is inevitably a thin B_2O_3 layer on the as-received B_4C particle surface [8]. A thicker B_2O_3 layer willform during the calcination of the hybrid preform. Due to its low melting point, 450 °C [9], the B_2O_3 on the surface of particles exists as a liquid during the infiltration of the preform. The liquid B_2O_3 might then react, from a thermodynamic point of view, with liquid magnesium or solid MgO in the matrix according to reactions described by Equations 2 to 4. These reactions could have important effects on interfacial composition and structure,

$$B_4C + 4O_2 = 2B_2O_3 + CO_2 \quad (1)$$

$$B_2O_{3(L)} + 4Mg_{(L)} = MgB_{2(S)} + 3MgO_{(S)} \quad (2)$$

$$B_2O_{3(L)} + 3Mg_{(L)} = 2B_{(S)} + 3MgO_{(S)} \quad (3)$$

$$B_2O_{3(L)} + 2MgO_{(S)} = Mg_2B_2O_{5(S)} \quad (4)$$

and hence wettability, nature and strength of the interfacial bonding, and successively the mechanical properties of the composite. However, studies on this aspect in magnesium-based composites are rather rare. In the present work, the oxidation behavior of B_4C was investigated by measuring the weight changes during isothermal heating at 650 to 800 °C. The interfacial microstructure of the B_4Cp and SiCw reinforced ZK60 hybrid composite was studied using TEM and EELS.

* Author to whom all correspondence should be addressed.

2. Experimental procedure

The matrix used in this investigation is a ZK60 magnesium alloy (6.0Zn, 0.5Zr). The reinforcement consists of 12 vol pct high purity B_4C particles of 7 μm average diameter and 12 vol pct SiC whisker of 0.5–1.5 μm diameter and 10–50 μm length. The hybrid technique enables the desired properties to be obtained by the appropriate combination of ceramic materials.

The oxidation behavior of the B_4C particles in air at different temperatures was determined by measurements of weight changes using a TG328A photoelectric balance. Crystal structure of the surface oxidation product was identified by X-ray diffraction using a Rigaku DMAX RX-10 diffractometer. Cu-K_α radiation was used and operated at 40 kV and 40 mA with a scanning rate of 4° min^{-1}. Morphologic observation of the as-received and oxidized particles was performed on a Philips SEM 515 scanning electron microscope.

The preforms of B_4C particles and SiC whiskers with small amount of binder were calcinated at 700 °C for two hours in order to obtain adequate strength. The composite billets were fabricated using the technique of pressure infiltration under vacuum. The processing parameters for the technique were: melt temperature 730 °C, preform temperature 650 °C, and the infiltration pressure 7 MPa. The billet was kept under this pressure for 10 minutes while its temperature decreased to about 550 °C. Afterwards, the billet was cooled to 300 °C in the furnace and then cooled to ambient temperature in air. The billet was then extruded under a deformation ratio of 16 : 1.

Specimens for TEM and EELS were cut from the as-extruded rod and prepared by standard methods involving mechanical grinding, polishing and dimpling followed by ion milling of foils to perforation on a liquid nitrogen-cooled specimen stage to eliminate further aging during the thinning period. Morphologic and structural studies were performed in a Philips CM12 analytical transmission electron microscope and operated at an acceleration voltage of 100 keV. An EDAX and a PV9900 X-ray spectrometer and a Gatan 666 parallel electron energy loss spectrometer are linked to the CM12 microscope.

Fractographic observation of the fractured samples was carried out on Philips SEM515 scanning electron microscope.

3. Results and discussion

3.1. Kinetic study of the oxidation of the B_4C particles

The activation energy for the oxidation from B_4C to B_2O_3 was measured in this work from the variation of reaction percentage of B_4C with temperature. The transformation kinetics were expressed by means of a Johnson-Mehl-Avrami-type relationship [10, 11]. Assuming volume diffusion is the controlling steps in the oxidation and at a constant reaction percentage of B_4C, the activation energy of diffusion, Q, for the reaction rate controlling species may be determined by plotting $\ln t$ vs $1/T$; that is,

$$\left[\frac{\partial \ln t}{\partial(1/T)}\right]_x = \frac{Q}{R} \tag{5}$$

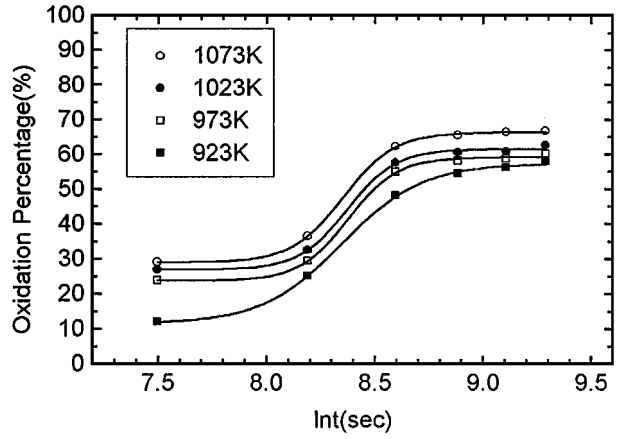

Figure 1 Plot of oxidation percentage vs. logarithm of time for the oxidation of B_4C to B_2O_3.

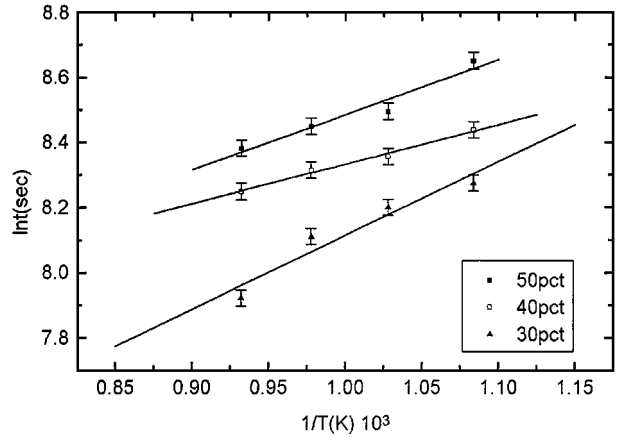

Figure 2 Plot of logarithm of time vs. reciprocal of temperature for the oxidation of B_4C to B_2O_3.

where t is the reaction time at a constant temperature T; x represents the reaction percentage of B_4C and R is the gas constant.

According to Equation 1, oxidation of one mole B_4C (55.2 grams) will produce two mole of B_2O_3 (2×69.6 grams). That is to say that when B_4C is oxidized thoroughly the corresponding weight gain will be 152.2% or 1% weight gain corresponds to the 0.657% oxidation of the B_4C. Therefore, the reaction percentage of B_4C can be determined based on the measurement of the weight gain. Fig. 1 is a plot of the logarithm of time vs. the reaction percentage of B_4C. Assuming a linear relationship between the successive data points, the time needed for the 30%, 40%, and 50% transformation of B_4C at different temperatures was determined from Fig. 1 and then plotted $\ln t$ vs. $1/T$ (Fig. 2). The slopes of these fitted lines represent the values of Q/R, which are 2267.3, 1213.6 and 1697.1 for 30%, 40% and 50% reaction, respectively. The average value of Q is 14.4 ± 4.4 KJ/mol. According to the physical process of the oxidation and the calculation model used, this value of Q represents the activation energy for oxygen diffusion in liquid B_2O_3. The kinetics of the oxidation of B_4C in air at 650 to 800 °C is thus limited to the diffusion rate of oxygen through the liquid B_2O_3 layer.

The X-ray diffraction pattern of the B_4C particles in the as-received and oxidized conditions are shown in

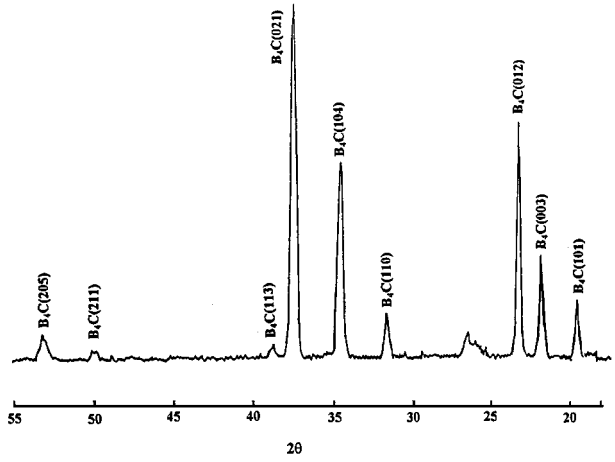

Figure 3 XRD pattern for as-received B_4C particles.

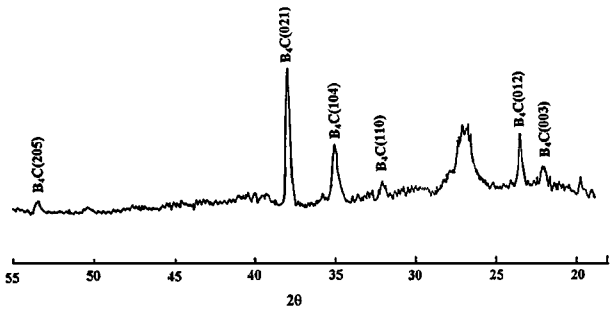

Figure 4 XRD pattern for B_4C particles oxidized at 800 °C for one hour.

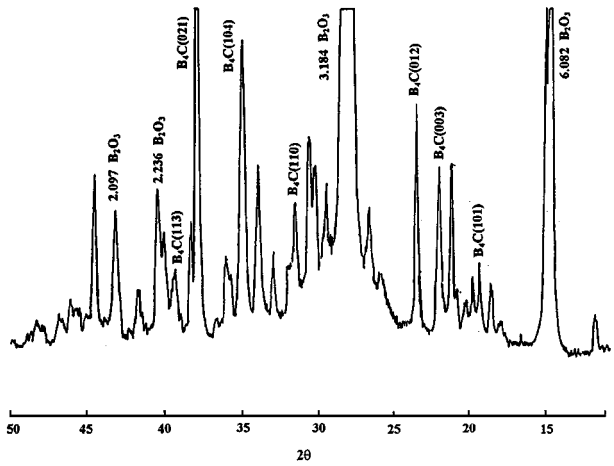

Figure 5 XRD pattern for B_4C particles oxidized at 800 °C for one hour and crystallized from hot water.

Figs 3 and 4, respectively. Fig. 3 has been indexed coincident with a rhombohedral structure with $a = 0.56$ nm and $c = 1.208$ nm. In comparison with Fig. 3, the intensity of the B_4C peaks in Fig. 4 are obviously decreased due to the oxidation of B_4C into B_2O_3. However, no any B_2O_3 peak is shown in the XRD pattern which indicates that B_2O_3 may be in an amorphous state. In order to verify further this judgment, B_4C particles oxidized at 800 °C for one hour were boiled in distilled water and then let water to evaporate at 90 °C. After drying the particles were subjected to XRD test. Sharp and strong peaks for B_2O_3 and B_4C are shown in the resulted pattern in Fig. 5. It indicates that the B_2O_3 formed by oxidation of B_4C in air is in an amorphous state. The B_2O_3 dissolves in hot water and then precipitates into crystalline.

3.2. Interfacial structure analyses

Typical TEM micrographs from the interface region between the B_4C particle and the Mg matrix are shown in Fig. 6a and b from which two kind reaction products with different morphologies, block-like and granular compounds, are clearly seen. Examinations using an energy-dispersive X-ray spectrometer (EDS) with a beryllium window showed that both compounds contained Mg. Further detection using EELS proved that boron existed in the block-like compound (Fig. 7) and oxygen existed in the granular shaped compound. In

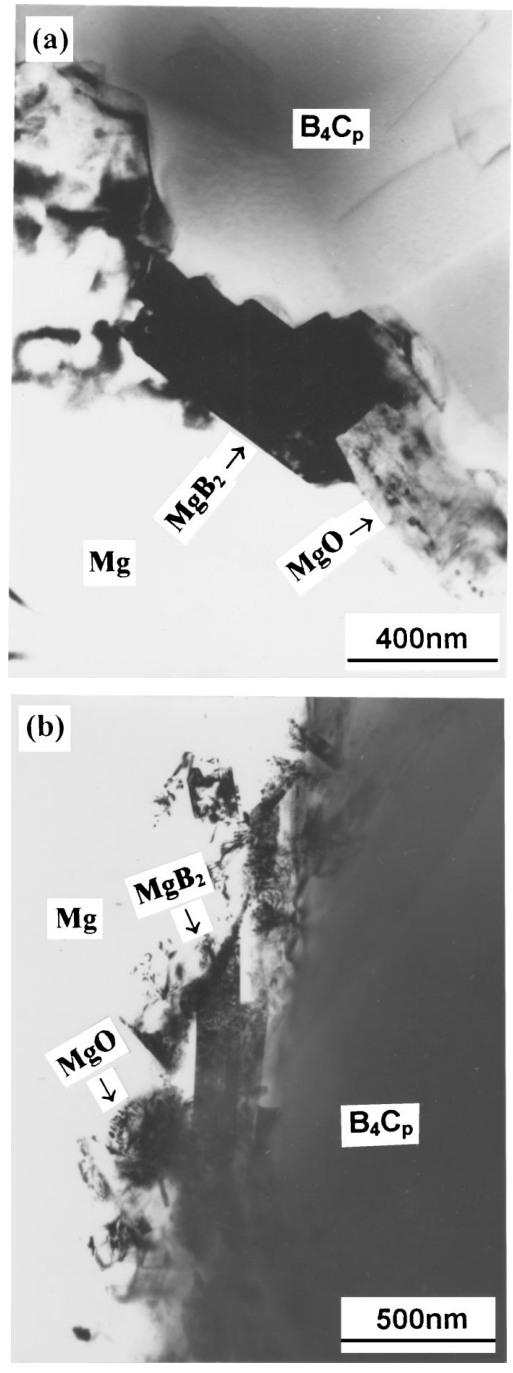

Figure 6 TEM micrograph showing interfacial reaction products with different morphology (a) block-like and granular reaction products (b) rod-like and granular reaction products.

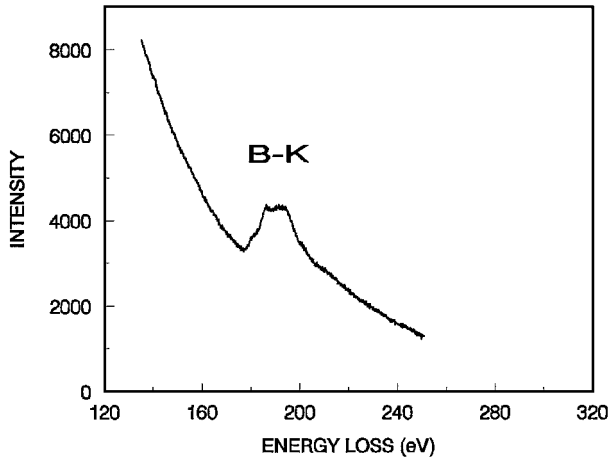

Figure 7 EELS spectrum showing existence of boron in the block-like compound in Fig. 6a.

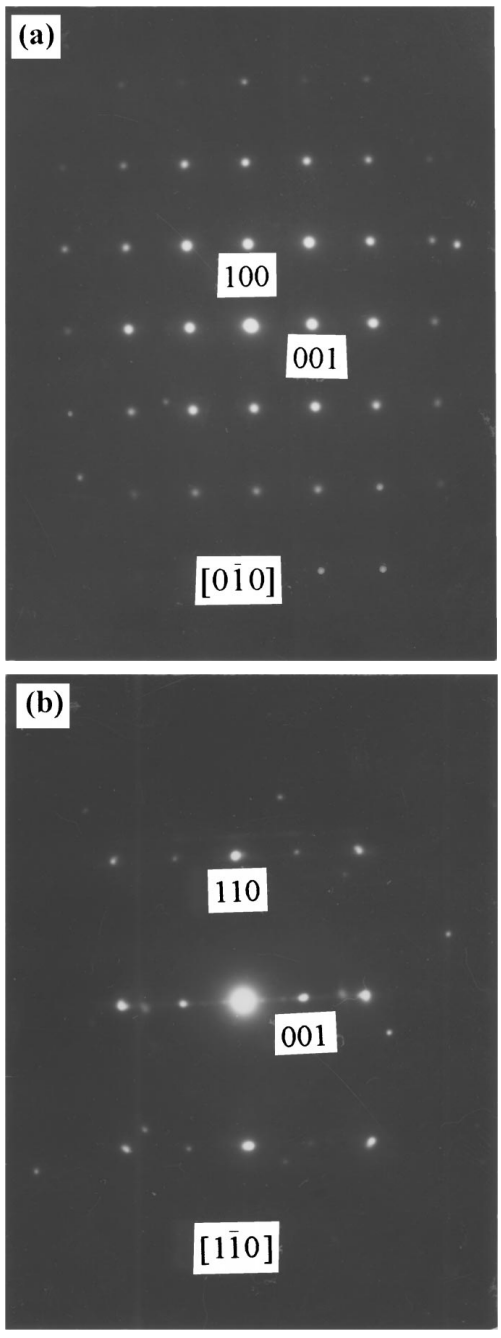

Figure 8 Selected area electron diffraction patterns obtained from the block-like compound in Fig. 6a which has been identified as MgB_2 (a) zone axis = [010]; (b) zone axis = [110].

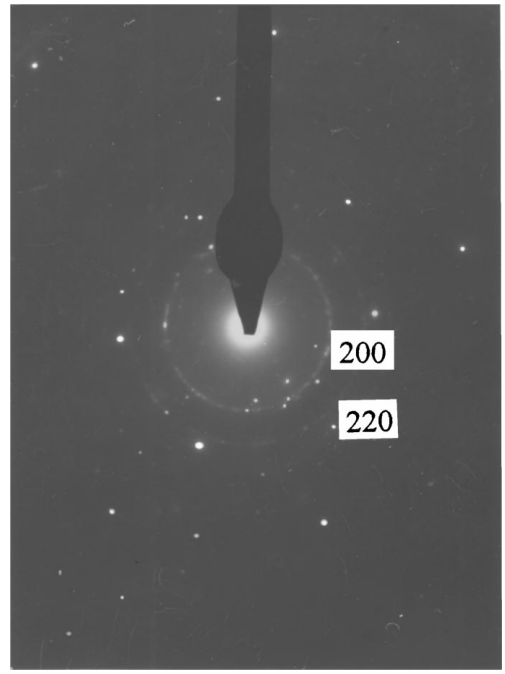

Figure 9 Selected area electron diffraction pattern obtained from the small granular particles in Fig. 6b which has been identified as MgO.

combination with the structural analysis on the selected area electron diffraction patterns in Figs 8 and 9, it is concluded that the block-like interfacial compound is MgB_2 and the granular shaped one is MgO. The sharp ring pattern of the MgO indicates that it is composed of very fine grains. Based on above analyses, it can be proposed that an oxidation layer has been formed on the B_4C particle surface although the calcination and preheating of the B_4C preform was taken place in a low vacuum of 10-1 torr (=13.3 MPa). In fact, it has been measured that the weight gain of the B_4C particles after being subjected to the same thermal process and under the same low vacuum as the preform is 2.5%. Therefore there is 1.64 weight percent B_2O_3 layer on the surface of the B_4C particles according to the above studying in the Section 3.1. This surface oxidation layer have reacted with liquid Mg matrix to form block-like crystalline MgB_2 and granular micro-crystalline MgO

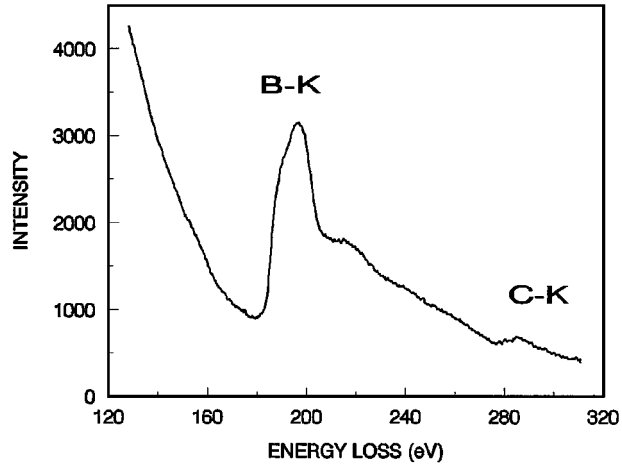

Figure 10 EELS spectrum showing existence of boron and carbon on the surface area of the B_4C particle in Fig. 6a.

according to the reaction described by Equation 2. Reactions in Equation 3 and 4 did not occur noticeably because neither B nor $Mg_2B_2O_5$ were found in all the samples observed.

The morphology of MgB_2 in Fig. 6a is different from that in Fig. 6b. In Fig. 6a the MgB_2 block is intimately bonded with the B_4C particle. In order to know whether or not a layer of B_2O_3 was remained between the MgB_2 and the B_4C, compositional and structural analyses were performed on the B_4C particle near the interface in Fig. 6a using EELS (Fig. 10) and ED (Fig. 11). Only boron and carbon were detected and the structure at the particle surface was still a rhombohedral with $a = 0.56$ nm and $c = 1.208$ nm after preform calcination and Mg infiltration. No Oxygen and residual B_2O_3 were found on the particle surface. This is understandable because the reaction during the infiltration process was taken place between two liquid phases and it should be rapid and completed. The facets between the MgB_2 block and the B_4C were proved to be (003) and (010) low indexing planes of B_4C through trace analyses. No definite crystallographic orientation relationship between the MgB_2 and the B_4C was found.

The MgB_2 rod was found apart from the B_4C surface in Fig. 6b. This is because the B_2O_3 was in a liquid state during infiltration [9]. The liquid B_2O_3 may flow away from the surface of the B_4C under the scouring of the liquid Mg. The liquid B_2O_3 could also flow to

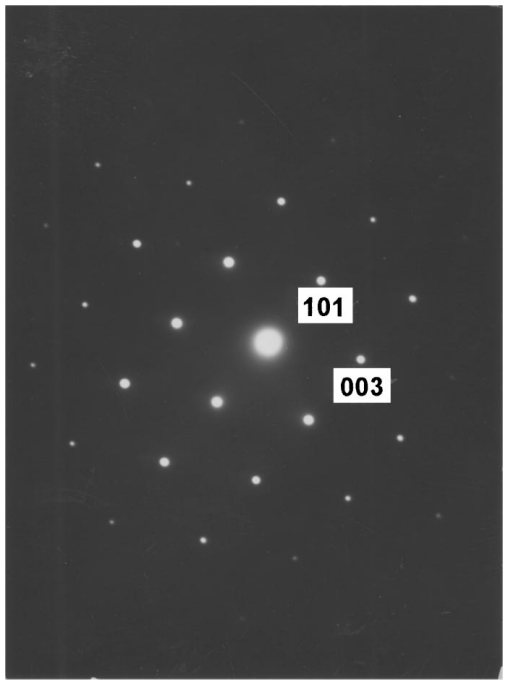

Figure 11 Selected area electron diffraction patterns obtained from the surface area of the B_4C particle in Fig. 6a which has been indexed as a rhombohedral structure with $a = 0.56$ nm and $c = 1.208$ nm. The zone axis = [010].

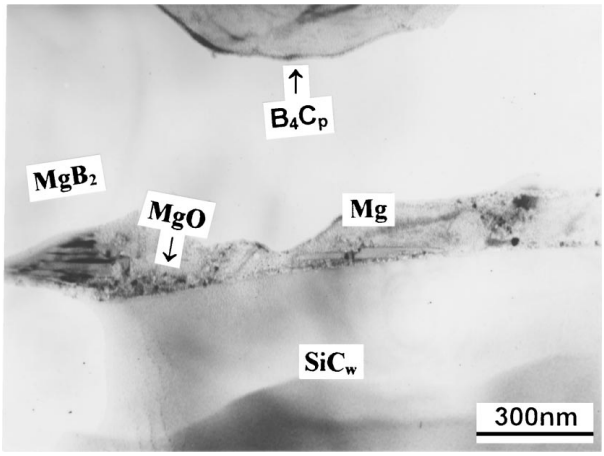

Figure 12 TEM micrograph showing interfacial compounds on the SiC whisker near a B_4C particle.

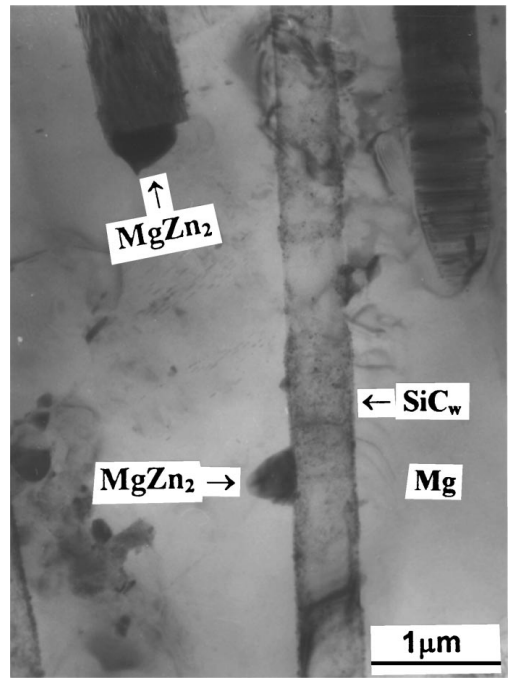

Figure 13 TEM micrograph showing interfacial compounds on the SiC whisker far from B_4C particles.

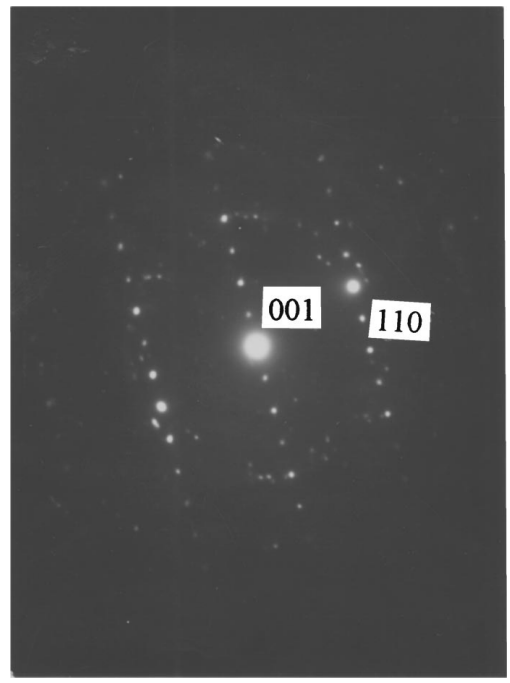

Figure 14 Selected area electron diffraction pattern obtained from the interfacial compound on the surface of the SiC whisker in Fig. 13. The pattern has been indexed as β' ($MgZn_2$) phase, zone axis = [110].

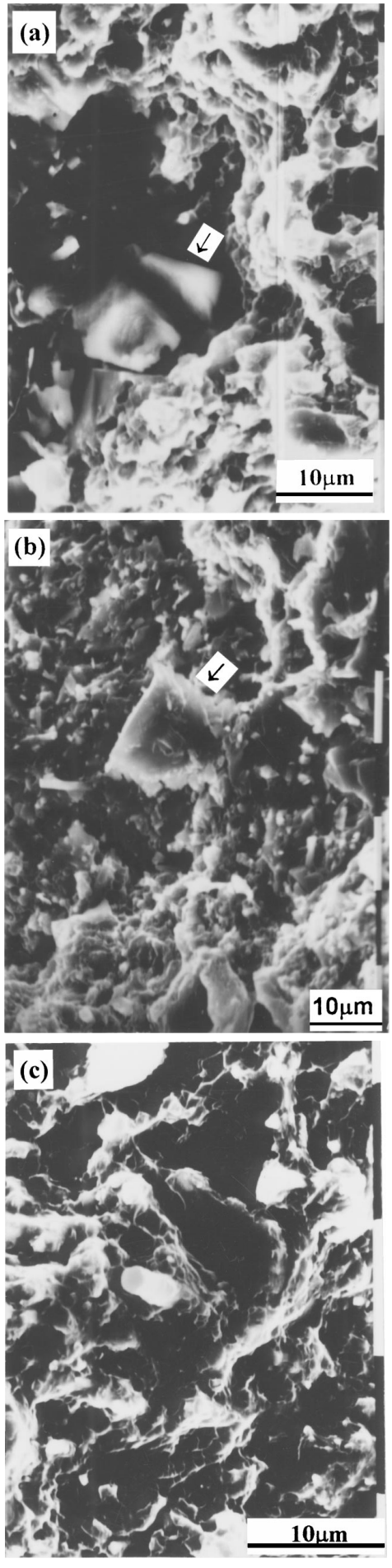

Figure 15 SEM fractographs of the composite showing (a) a cracked B_4C particle; (b) a thin layer of matrix adherent to a B_4C particle; (c) a pull-out SiC whisker.

the SiC whisker near the B_4C particle and then form MgB_2 and MgO on the whisker surface (Fig. 12). Typical morphology of the interfacial compound on the surface of SiC whiskers which are far from B_4C particulates is shown in Fig. 13. The compound in this micrograph was identified as $\beta'(MgZn_2)$ using EDX and ED (Fig. 14). β' is formed due to the macrosegregation during the infiltration solidification of ZK60 alloy matrix. Macrosegregation during infiltration, featuring significant solute enrichment at the infiltration front, occurs because solute is partitioned unequally between liquid and solid during solidification [12]. EDS and EELS detections in the vicinity of the interfaces between the SiC whisker and the Mg matrix indicated that no detectable interdiffusion and chemical reaction occurred between the elements in the whisker and the matrix. This is in accordance with the previous results that SiC is stable enough in the Mg-Zn alloy [7, 13].

Results of the mechanical property study of the present composite in the as-extruded state has been reported elsewhere [4]. The reported tensile strength and elastic modulus for the composite are 419.4 MPa and 80.6 GPa, which are 53% and 110% higher than those for the unreinforced ZK60 alloy, respectively. Fractography was performed on the fractured tensile specimens to explore the reasons responsible for the improvement of mechanical properties. It is shown that particle cracking is popular on the fracture surface (Fig. 15a) and a matrix layer is often detected on the surface of B_4C particles (Fig. 15b). Many small rods can be seen in the figure which stick into the matrix layer. Debonding of the particle/matrix interface was seldom seen on the fracture surface. Only slight pull-out of the SiC whiskers was found on the fracture surface area without concentrated particles (Fig. 15c). These features suggest that cracking took place in the B_4C particles and in the matrix near the matrix/particle interface where the fracture strength factor is maximum. Strong interfacial bonding between the particle and the matrix are partly due to the presence of the rod-like MgB_2 which stick in the matrix tightly. It is generally accepted that strong particle/matrix interfacial bonding is beneficial to the load transfer and hence to the tensile strength of a composite material [14]. In addition, the strong bonding between the whiskers/matrix which was manifested by the shortage of fiber-pull-out also enhanced the strengthening effect of the whisker, however, a considerable decrease in ductility was associated.

4. Conclusions

1. The oxidation of B_4C particles in air at 650–800 °C produced an amorphous B_2O_3 surface layer. The oxidation kinetics was limited by the diffusion rate of the oxygen through the liquid B_2O_3 layer.

2. The B_4C particles are stable in the matrix of ZK60 alloy. However, due to the presence of a B_2O_3 surface layer which formed during the calcination and preheating processes of the reinforcement preform, interfacial reactions occurred between the B_2O_3 and the Mg and produced the rod-like MgB_2 and the granular MgO.

3. No reaction between the SiC whiskers and molten magnesium was observed. The MgB_2 and MgO existing

on the whisker surfaces were the reaction products between the Mg and the B_2O_3 which flowed on to the whisker surfaces from the surface of B_4C particles.

4. Crackings were mainly observed in particles and in the matrix ahead of the particle/matrix interfaces. The intimate bonding of the MgB_2 with reinforcements and with the matrix is beneficial to the strengthening of the composite.

Acknowledgements

Financial support of this work from the National Natural Science Foundation of China are grateful. One of the author, Mingyuan Gu, would also like to thank the DFG of Germany for the financial support of his visiting in GKSS Research Center.

References

1. H. J. RACK and P. W. NISKANEN, *Light Metal Age* **42**(1/2) (1984) 9.
2. YASUYUKI INOSE, JUNICHI KANEKO and MAKOTO SUGAMATA, *Light Metal* (in Japanese), **40** (1990) 221.
3. J. SCHRÖDER and K. U. KAINER, *Mater. Sci. Eng.* **A135** (1991) 33.
4. J. L. QIN, G. D. ZHANG, D. ZHANG and H. M. WANG, in Proceedings of the 2nd Annual Meeting of the Chinese Aeronautical Society, October 1997, Shanghai, p. 134.
5. C. BADINI, F. MARINO, M. MONTORSI and X. B. GUO, *Mater. Sci. Eng.* **A157** (1992) 53.
6. R. F. VOJTOVICH, in 'Oxidation of Carbides and Nitrides,' Naukova Dumka, Kiev, 1981.
7. S.-Y. OH, J. A. CORNIE and K. C. RUSSELL, *Metall. Transactions* **20A** (1989) 533.
8. V. A. LAVRENKO and Y. G. GOGOTSI, *Oxidation of Metals* **29** (1988) 193.
9. C. T. LYNCH, "CRC Handbook of Materials Science, Vol. I: General Properties," (CRC Press Inc., Boca Baton, Florida, 1984), p. 348.
10. W. A. JOHNSON and R. F. MEHL, *Trans. AIME* **135** (1939) 416.
11. M. AVRAMI, *J. Chem. Phys.* **9** (1941) 177.
12. A. MORTENSEN and I. JIN, *Int. Mater. Rev.* **37**(3) (1992) 101.
13. P. K. CHAUDHURY, H. J. RACK and B. A. MIKUCKI, *J. Mat. Sci.* **26** (1991) 2343.
14. NING WANG, ZHIRUI WANG and G. C. WEATHERLY, *Metall. Trans.* **23A** (1992) 1423.
15. B. INEM and G. POLLARD, *J. Mater. Sci.* **28** (1993) 4427.

Received 2 March
and accepted 22 October 1999